Materialia 12 (2020) 100709

Contents lists available at ScienceDirect

Materialia

journal homepage: www.elsevier.com/locate/mtla

Full Length Article

Silk fibroin magnetoactive nanocomposite films and membranes for dynamic bone tissue engineering strategies

A. Reizabal[a,b], R. Brito-Pereira[c,d], M.M. Fernandes[c,e,*], N. Castro[a], V. Correia[f], C. Ribeiro[c,e], C.M. Costa[c,g], L. Perez[a,b], J.L. Vilas[a,b], S. Lanceros-Méndez[a,h,*]

[a] BCMaterials, Basque Center for Materials, Applications and Nanostructures, UPV/EHU Science Park, 48940 Leioa, Spain
[b] Departamento de Química Física, Facultad de Ciencia Y Tecnología, Universidad del País Vasco/EHU, Apdo. 644, Bilbao, Spain
[c] Centre of Physics, University of Minho, 4710-057 Braga, Portugal
[d] CMEMS-UMinho Research Unit, University of Minho, Guimarães, Portugal
[e] Centre of Biological Engineering, University of Minho, Campus de Gualtar, Braga 4710-057, Portugal
[f] Centro Algoritmi, Universidade do Minho, Campus de Azurém, 4800-058 Guimarães, Portugal
[g] Centre of Chemistry, University of Minho, 4710-057 Braga, Portugal
[h] Ikerbasque, Basque Foundation for Science, 48013 Bilbao, Spain

ARTICLE INFO

Keywords:
Silk-fibroin
Magnetic nanoparticles
Magnetic stimulation
Biomedical application
Tissue engineering

ABSTRACT

Bone-related diseases are one of the most common health conditions that limit the quality of life of elderly. Novel materials for bone tissue engineering that actively assist on the regeneration of bone tissue are thus needed. In this work, magnetoactive scaffolds comprised of silk fibroin (SF) with different content of filler – cobalt ferrite nanoparticles – were produced by solvent-casting and electrospinning technique and further evaluated for bone cells growth under static and dynamic magnetic stimulation. The materials were evaluated for their enhanced electric properties, analyzed through the silk fibroin β-sheet content, an important factor for the envisaged cell stimulation strategy, which are in much higher content in films (~50%) than in electrospun fibers (~25%). Cell culture experiments under varying magnetic field, induced a magneto-mechanical stimulation on the materials, hence on cells, promoting improved cell viability after 4 days of culture. The scaffold morphology was found to play an important role in pre-osteoblast proliferation rate, being larger for cells growing on films, which is related to the topography of the material but also to the increased β-sheet content. It is shown that the use of magnetic cues on magnetoactive biocompatible scaffolds is a promising strategy for remote stimulation of bone for its regeneration.

Statement of Significance

The use of physical stimuli such as electrical and mechanical cues have been proven a powerful tool for bone tissue engineering applications, but the use of magnetic cues on magnetoactive scaffolds has been scarcely reported. This is considered a promising strategy for remote stimulation of bone for its regeneration. The present study provides data on the evaluation of biocompatible silk fibroin scaffolds for bone cells' proper adhesion and proliferation upon the application of a magnetic stimuli using a custom-made magnetic bioreactor. The conditions created promote a biomimetic microenvironment through the application of a mechanical and electrical cues to cells. This approach is interesting since while scaffolds mimics the morphology of bone, the magnetic bioreactor provides the physical environment of bone, i.e. piezoelectricity, by generating electrical and mechanical cues with magnetic stimulation.

1. Introduction

Materials that are environmentally friendly, biocompatible and biodegradable is a common requirement for applications in specific areas such as biomedical and tissue engineering. Usually, these materials intend to target biomimetic approaches, by imitating the properties of human tissues and thus improve cellular response outcome [1,2] Scaffolds based on natural polymers such as silk, have been widely used

* Corresponding authors at: Centre of Physics, University of Minho, 4710-057 Braga, Portugal.
E-mail address: margaridafernandes@fisica.uminho.pt (M.M. Fernandes).

https://doi.org/10.1016/j.mtla.2020.100709
Received 1 February 2020; Accepted 30 April 2020
Available online 19 May 2020

for such purposes, since it typically hold biocompatibility, biodegradability and specific biological cues recognized by cells for physiological processes, offering to the cells a recognizable environment for proliferation and tissue remodeling [3]. Indeed, silk is being reinvented as biomaterial due to their unique mechanical properties [4], opportunities for genetically tailoring its structure and function [5], biocompatibility and intrinsic piezoelectricity [6], an important factor since bone itself is piezoelectric.

This natural biopolymer is constituted by silk fibroin (SF), a typical fibrous protein that forms the filaments of silkworm cocoon, *Bombyx mori,* and is formed by the amino acids glycine (45%), alanine (30%) and serine (12%) in a 3:2:1 ratio and dominated by [Gly-Ala-Gly-Ala-Gly-Serl]$_n$ sequences, leading to an antiparallel β-pleated sheet formation in the fibers [4,7,8]. Silk sericin is the other main protein present in the silks constitution, representing the water-soluble glue-like protein that bind the fibroin fibers together [9]. Increasing attention is devoted to SF electrospun scaffolds in the biomedical field, particularly for wound healing applications [10], since fibroin possess unique properties for skin regeneration including biocompatibility, enhanced collagen biosynthesis, minimal immunogenicity, anti-inflammatory activity, an haemostatic activity [11,12]. Thus, SF electrospun fibers are valuable due to their nontoxic and biodegradable nature as well as for actively supporting the regeneration of healthy tissues [13].

In fact, electrospinning can produce a diverse range of polymer nanofibers diameters and structures determined by the polymer and the processing conditions [14]. The electrospinning process consists in the application of a high voltage in order to create jets of a polymer solution that upon drying form nanofibers that are collected on a static or dynamic target [15]. The tunable and controllable nature of electrospinning makes it a highly efficient scaffold fabrication technique [16]. Properties such as fiber diameter and alignment, porosity and high surface area are highly interesting for biomedical applications [17]. Once processed in the specific range of diameters, the fibers in a (micro/nano scale) may simulate the extracellular matrix (ECM) and then, afford mechanical and structural support to cells, improving cell proliferation and migration [18]. In agreement with this aspect, the surface texture and morphology has an important effect in the control of cell adhesion, migration, growth, proliferation, function and shape [19,20]. Nonwoven fabrics with an optimized surface microstructure are among the most promising material forms used in tissue engineering, due to their porous three dimensional structure and the high specific surface area desirable for high-density cell and tissue cultures [21,22]. Further, electrospinning also allows the processing of materials with combined properties. One such example is the development of nanocomposites comprising magnetic nanoparticles. These magnetic responsive materials have been a focus of interest in tissue engineering [23], biosensors or microfluidics [24], due their controlled response and reproducibility [24]. In particular, cobalt ferrite nanoparticles are characterized by high magnetization properties and high magnetostrictive response, and have already been successfully used for the formulation of silk-based non-cytotoxic magnetic biocomposites [25]. In addition to the incorporation of magnetic properties, the incorporation of particles within the electrospun silk matrix, the intrinsic piezoelectricity of silk fibroin had already showed promising results in sensors [26], drug delivery or when applied to bone cells due to the biomimetic intrinsic piezoelectric mechanism of bone and by promoting a proper microenvironment for the efficient growth and proliferation of these tissues [27]. In fact, the interest and suitability of piezoelectric stimulation for tissue engineering has been mainly investigated with synthetic polymers such as poly(vinylidene fluoride) (PVDF) [28]. The piezoelectric response of PVDF and PVDF nanocomposites incorporated with CFO fillers, to a mechanical and magnetic stimulus, respectively, and its effect response for bone cell stimulation has been reported under static and dynamic mechanical stimuli [29,30]. Despite the promising results, there are some features that need to be addresses namely the fact that synthetic polymer scaffolds show poor capability of cell attachment due to the lack of cell recognition sites in comparison to natural biopolymers [31]. Thus, encouraged by the potential applications of silk fibroin magnetic composite scaffolds, the present study analyzes the physico-chemical and magnetic properties of SF composites processed with different designs (films and fibers) and at varying concentrations of $CoFe_2O_4$ nanoparticles, as well as it evaluates the applicability of these nanocomposites for bone tissue engineering.

2. Experimental

2.1. Materials

Bombyx mori silkworm cocoons were supplied by APPECDM from Castello Branco (Portugal). Na_2CO_3, formic acid and calcium chloride ($CaCl_2$) were obtained from Sigma-Aldrich and were used as received. Cobalt ferrite – $CoFe_2O_4$ (CFO) round magnetic NPs with 35–55 nm diameter were purchased from Nanoamor.

2.2. Silk fibroin extraction and solution

Silk fibroin was extracted from Bombyx mori silkworm cocoons by a standard method, also named soap degumming [26]. Thus, non-damaged cocoons were selected, cleaned and cut in 1 cm^2 pieces. Cocoons were then boiled in 0.05 wt%. Na_2CO_3 water solution for 30 min in a silk to water solution ratio (w/v) of 1:40. The resultant solid fibers of silk fibroin were cleaned through abundant distilled water and dried at room temperature for 24 h. Silk fibroin solution for film and electrospun membrane preparation was prepared in a two-step process. Silk fibroin fibers were initially dissolved in a 0.17 M solution of FA/$CaCl_2$ in a ratio of 12:1 v/w (formic acid:SF). In order to remove impurities, solution was centrifuged at 7500 rpm during 10 min. The resultant SF/FA/$CaCl_2$ solution was cast at room temperature for 24 h to remove the FA. The resultant transparent and plastic material was cleaned in distilled water bath to remove the $CaCl_2$ and dried at room temperature, leading to brittle and whitish SF. In a second step, SF was dissolved in neat FA (5:1 v/w FA:SF) in order to obtain a SF/FA solution suitable for film and membranes preparation.

2.3. SF films and membranes preparation

SF films and membranes were prepared following the main steps represented in Fig. 1. SF/CFO films with 5%, 10% and 20% CFO content are named as SFF-5, SFF-10 and SFF-20 respectively. SF/CFO membranes of 5%, 10% and 20% CFO content are named SFM-5, SFM-10, SFM-20. Films and membranes precursory solution was prepared by mixing two different solutions, the first one described ahead and a second one composed by CFO NPs dispersed in FA by 1.5 h of ultrasonication. In order to obtain a solution with the adequate viscosity, CFO NPs were dispersed in the same volume in which the SF was dissolved. Both solutions were then mixed in a vortex mixer MX-S during 5 min to obtain a SF/CFO solution (10:1 w:w). Due to the chemical stability of the CFO NPs, no variation occurs during the processing of the films and membranes [32].

SF/CFO films with a thickness of 40–60 μm were obtained by casting the final solution over polyethylene petri dishes for 24 h at room temperature. Neat SF films were prepared following the same steps without CFO NPs addition.

SF/CFO membranes were obtained by electrospinning technique. The SF/CFO solution was electrospun with a syringe connected to a HiTeh Power station Series 400. The syringe diameter was 0.8 mm, the distance to the collector was 20 cm, and power source parameters were 20 kV and 0.01 mA. Membranes with a thickness of 0.5 mm were prepared of both pristine SF and SF/CFO composites.

2.4. Physical-chemical characterization

Atomic Force Microscopy (AFM) measurements were performed by CSInstruments in order to study the morphology of SF/CFO nanocom-

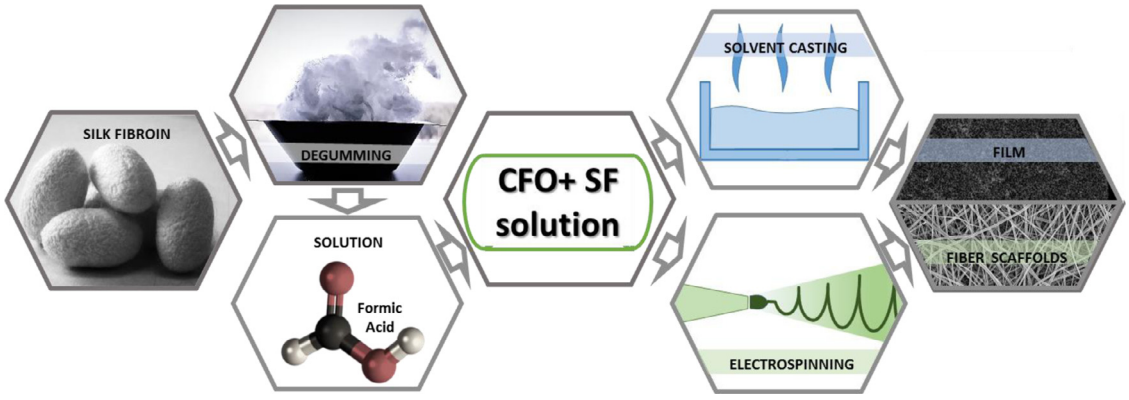

Fig. 1. Schematic representation of SF/CFO based films and membranes processing procedure.

posites. Measurements were collected in 8 μm side squares at 0.25 lines per second and a resolution of 512 lines per side at room temperature. In order to avoid membranes damage and AFM tangling, non-contact resonant mode was used with frequency of 73 kHz and amplitude of 84°.

The morphology of the SF/CFO nanocomposites were examined using a scanning electron microscope (SEM, NanoSEM – FEI Nova 200 (FEG/SEM)) with an accelerating voltage of 15 kV.

Attenuated Total Reflectance (ATR) Fourier Transform infrared (FTIR) spectroscopy was used to study the secondary structure of SF nanocomposites with a Jasco FT/IR-4100 system. Data were collected at room temperature from 4000 to 600 cm^{-1} using 64 scans at a resolution of 4 cm^{-1}. The determination of beta-sheet content was performed by Amide I region deconvolution [33]. Thermal Gravimetric Analyzer (TGA) – TGA/SDTA 851e Metter Toledo apparatus- was used to analyze the thermal degradation of the samples in the temperature range of 25 to 800 °C with a heating rate of 10 °C min^{-1} under constant air flow.

Differential scanning calorimetry (DSC) –Mettler Toledo DSC 822e equipment – was used to analyze the thermal transitions of the samples. Calorimetric scans were performed from 25 to 350 °C at a heating rate of 10 °C min^{-1} under nitrogen purge (50 mL min^{-1}). In order to remove the solvent lost endothermic peak, a first heating from 25 to 170 °C was performed.

Mechanical characteristics were analyzed by tensile testing using a Metrotech MTE-1 from Techlab system. Stress-strain tests were performed in specimens of 10 × 4 mm measured at 5 mm min^{-1} at room temperature. Young modulus was obtained from the slope of the characteristic curves between 0.5 and 1.5% strain in the stress–strain plots. Results show the mean obtained from 3 measurements.

Vibrating sample magnetometry (VSM) – EZ7 from MicroSense apparatus – was used to study the magnetic behavior of the SF/CFO nanocomposites between −1.8 and 1.8 T at room temperature.

2.5. Cell culture

MC3T3-E1 pre-osteoblast cells obtained from Riken Bank were used in all cell tests. The cells were maintained in Dulbecco's Modified Eagle's Medium (DMEM, Gibco) containing 1 g L^{-1} glucose, 10% Fetal Bovine Serum (FBS, Biochrom) and 1% penicillin/streptomycin (P/S, Biochrom) at 37 °C, in a humidified atmosphere with 5% CO_2, according to the recommendations of the manufacturer. The culture medium was replaced every 2 days. At pre-confluence, cells were harvested using trypsin-EDTA (Biochrom).

Preparation of the scaffolds: The different silk-based films and electrospun membranes were cut in circular samples with a diameter of 0.6 cm and sterilized using UV light for 1 h each side. The samples were then placed at the bottom of each well of a 48-well tissue culture polystyrene plate (Nunc).

Biocompatibility assays: The biocompatibility of the samples was determined by placing the pre-osteoblasts cells directly in contact with the surface of the material and by measuring the cell viability using 3-(4,5-dimethylthiazol-2-yl)-5-(3-carboxymethoxyphenyl)-2-(4-sulfophenyl)-2H-tetrazolium (MTS, Promega) assay at defined timepoints of 24 h, 4 days and 7 days. To avoid cell seeding on the plate rather than on the material, 35 μL of DMEM containing 15,000 cells (cell density = 40 × 10^4 cells mL^{-1}) were first placed on the surface of the material for 30 min and then 250 μL DMEM was added to the well (drop method – Fig. 2). MTS assay was then performed to determine cell viability and consequently the biocompatibility of the scaffold [28]. For this assay, after each time point, the samples were transferred to a new 48-well plate, MTS solution (in a 1:5 ratio) was added to each well and the plate was placed in a 5% CO_2 incubator at 37 °C. After 2 h of incubation, 100 μL of each well were transferred to a 96-well plate ($n = 3$) and the optical density (OD) of each well was measured at 490 nm using a spectrophotometric plate reader (Biotech Synergy HT). The quantitative results were obtained from three independent experiments and analyzed as the average of viability ± standard deviation (SD).

Cell culture assays in static and dynamic modes: Pre-osteoblast cells were seeded on the top of each sample using the above-mentioned drop method and two 48-well plates with the samples were prepared and incubated for 24 h. After this incubation time, one plate was maintained at the same conditions (static culture – cell culture without any applied stimuli) and the other was transferred onto a home-made bioreactor system (dynamic culture – cell culture under magnetic stimulation, i.e. varying magnetic field) for up to 4 days with the following cycle: an active time of 16 h under magnetic stimulus (divided into 5 min of active time and 25 min of resting time) followed by a non-active time of 8 h (non-magnetic stimulation) [29]. These conditions were selected in order to mimic the human body mechanical stimulations (16 h of activity and 8 h resting time) (Fig. 2) [34].

The dynamic cell culture was performed under magnetic stimulation at a frequency of 0.3 Hz. The 15 mm displacement of the permanent magnets below the culture wells allowed the variation of the magnetic field from a maximum value of 230 Oe to 0 Oe within the culture wells, leading to magnetomechanical stimulation of the scaffolds due to the magnetrostriction of the magnetic nanoparticles [29,35] and to eventual local variations of the electrical potential based on the piezoelectricity of silk fibroin [6]. In each study, 5 replicates were used per studied conditions. The viability of cells growing on the top of the material was assessed using the MTS assay and the proliferation rate was calculated in relation to the cell grown over the material after 24 h using the following equation.

$$Proliferation\ rate\ (\%) = \left[\left(\frac{Abs\ sample\ 4\ days_{490nm}}{Abs\ adhesion\ 24h_{490nm}}\right) x\ 100\right] - 100 \quad (1)$$

The morphology of the cells on the top of the materials was further analyzed using a desktop Scanning Electron Microscope (SEM) (Phenom

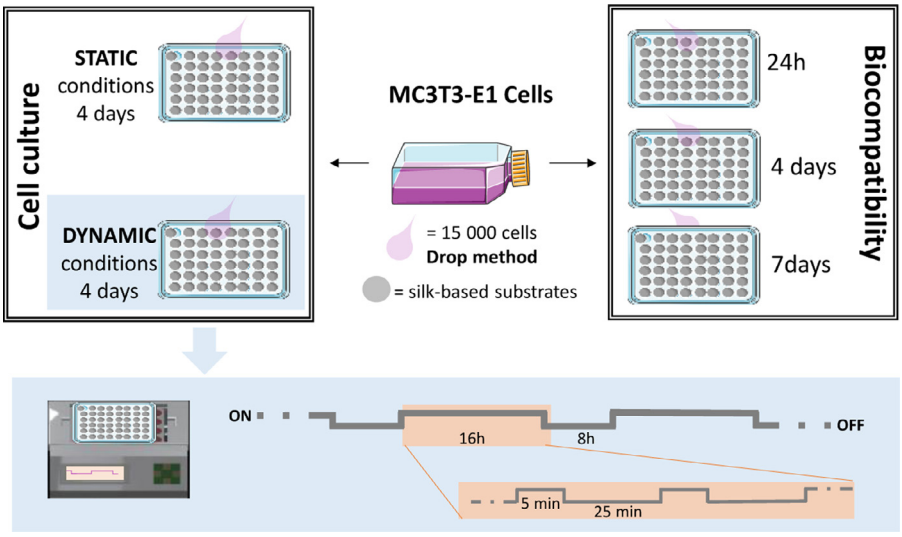

Fig. 2. Schematic representation of the cell culture assays using either static or dynamic conditions (magnetic stimulation). Below: time dependence of the dynamic magnetic stimulation.

ProX, Netherlands), after fixing and dehydrating the sample. Briefly, the samples were collected and transferred for a new 48-well plate, washed twice with PBS 1× and the cells fixed with 4% formaldehyde (Panreac) for 10 min at 37 ˚C in a 5% CO_2 incubator. Following the fixation of the samples, they were dehydrated by immersing the samples to solutions with increasing ethanol content: 25%, 50%, 70%, 90%, 95%, and absolute ethanol for at least 10 min. The material was then sputter-coated with gold with a thickness of 20 Angstrom and the images acquired using the ProSuite software. The samples were added to aluminum pin stubs with electrically conductive carbon adhesive tape (PELCO Tabs^{TM}) on a Phenom Standard Sample Holder (SH).

2.6. Data analysis

The quantitative results obtained from each sample are presented as averages with the corresponding standard deviations. Results were analyzed by Graph Pad Prism Version X for Windows (Graph Pad Software, San Diego, CA, U.S.A.). Statistical significance was determined by one-way ANOVA, followed by the unpaired two-tailed Student's *t*-test method.

3. Results and discussion

3.1. Morphological analysis

The morphology and roughness of the scaffolds is one of the most important parameters influencing cell activity [36] based on the mechanism of cell mechano-transduction phenomenon [37]. SF films and membranes morphology and roughness were analyzed by Atomic Force Measurements (AFM), as presented in Fig. 3(a). As the morphology of the films and membranes is influenced by the presence of the CFO NPs, the data from the SFF-20 and SFM-20 samples are used as representative for all samples.

The different processing techniques used to obtain films and membranes result in quite different morphologies. SF films show a smooth and compact surface with dispersed CFO NPs, no apparent fractures, and a small average roughness of 100 nm roughness (Fig. 3(b)). This morphology is explained by the solvent evaporation rates in the preparation of the films. The casting process of SF films from a solution with high solvent content (silk solvent ratio of 1:20 w:v) and solvent evaporation at room temperatures ensures slow solvent evaporation, avoiding Marangoni instabilities, which are commonly responsible of large films roughness [38]. The resulting film roughness includes irregularities of 3–10 nm in depth and less than 100 nm in width. Along the surface of the SF films, it is observed the presence of CFO NPs that make increase the surface roughness as CFO NPs content is increased.

On the other hand, the electrospun membranes are characterized by a nonwoven structure formed by randomly distributed SF fibers of 800 to 900 nm in diameter, forming a three-dimensional porous structure (Fig. 3). As for the films, CFO NPs are found on the fibers surface encapsulated by a thin polymer layer that enables (it will be shown latter) the non-cytotoxicity of the samples. AFM images reveal a multifibrillar structure since individual fibers are composed by closely packed smaller fibers of 200–300 nm.

In the electrospinning process, once the initial single jet is formed and elongated by the effect of electrical forces [39], physical instability processes related to Maxwell stresses and surface tensions, lead to the breakdown of the single jet static equilibrium, jet to undulatio [40] and induced tensions along the jet. In those sections where tensions are accumulated, and once the surface solution tension is exceeded, continuous lateral branches are formed and elongated by electrostatic forces [41], leading to lateral fibers that join together packing in larger fibbers which are finally deposited in the collector, as observed in Fig. 3. Fibers roughness show similar values as the ones observed for the films and it is also independent of the CFO NPs content.

3.2. Physical-chemical characterization

FTIR analysis allows to determine the effect at a molecular level of the different processing methods as well as that derived from CFO NPs addition. The FTIR data of SFF, SFF-20, SFM and SFM-20 are represented in Fig. 4. Amide I curves are thus shown in Fig. 4(a) as the most relevant FTIR spectral range in order to analyze the secondary structure of SF. Fig. 4(b) shows the vibrational band assignments for the main secondary structures of SF obtained from the deconvolution of the amide I region: side chains (SC), β-Sheets (β), random coil (RC), α-helix (A) and turns (T).

Regardless of the SF morphology and CFO addition and content, the main absorption bands of SF are clearly observed in all SF samples (supporting information – Fig. S1) suggesting that no relevant modifications of the primary structure of SF exists due to the selected processing methods due to the incorporation of the CFO NPs. In contrast, amide I data (Fig. 4(a)), regardless of the CFO addition, show large variations depending on the morphology, this is indicative of a change in the secondary structure due to the processing method. The vibrational band assignments obtained from the amide I deconvolution were used in order to quantify the observed effect (Fig. 4(b)). Slow solvent evaporation leads to improved polymer chain organization and therefore leading to a

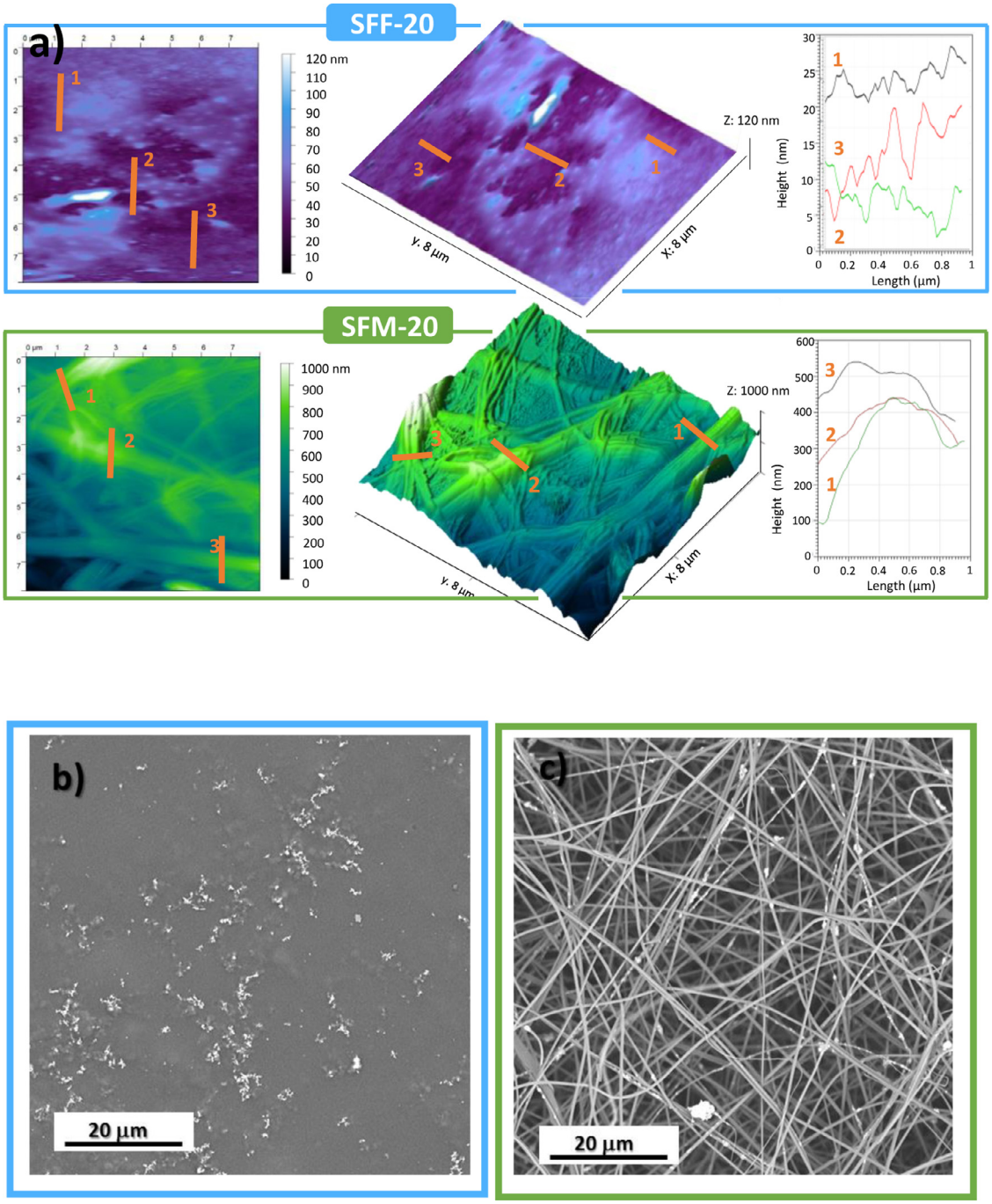

Fig. 3. (a) AFM images and surface topography measurements of SFF-20 (up) and SFM-20 (down) samples. The numbers 1, 2 and 3 represent three different scans for the determination of the average roughness of the samples. (b,c) SEM images of SFF-20 and SFM-20 samples, respectively.

highly crystallized structure [42], therefore, the solvent casting process resulted in a highly ordered SF structure with β-sheet contents above 50% and low α-helix and random coil content. Although incorporation of CFO NPs in the SF film also leads to structures dominated by β-Sheets (>45%), a slight decrease in β-Sheets content could be observed. Diminished ordered structure content suggests the hindering effect of NPs on the SF crystallization processes [25]. CFO NPs interact with the amine groups forming functional coatings [43,44], avoiding the free movement of the backbone and consequently, reducing the formation of ordered domains.

Neat SF membranes (Fig. 4(a) and (b)), on the contrary, show a secondary structure with low β-sheet (<25%) and high random coil and α-helix content. This result is related with the fast solvent evaporation rates during the spinning process, which leaves shorter times for the polypeptide repetitive sections to reorganize into β-sheet. Consequently, the non-ordered chains sections remain as random coils (amorphous phase). The increased amount of α-helix indicates that these structures are preferably formed when formic acid quickly leave the SF structure. SFM secondary structures are not significantly altered as a result of the addition of CFO NPs, suggesting that the hindering effect of NPs on the β-sheet is lower with respect to the effect of fast solvent evaporation.

The TGA results presented in Fig. 4(c) show the thermal degradation processes of the different SF samples. Neat SF films are characterized by

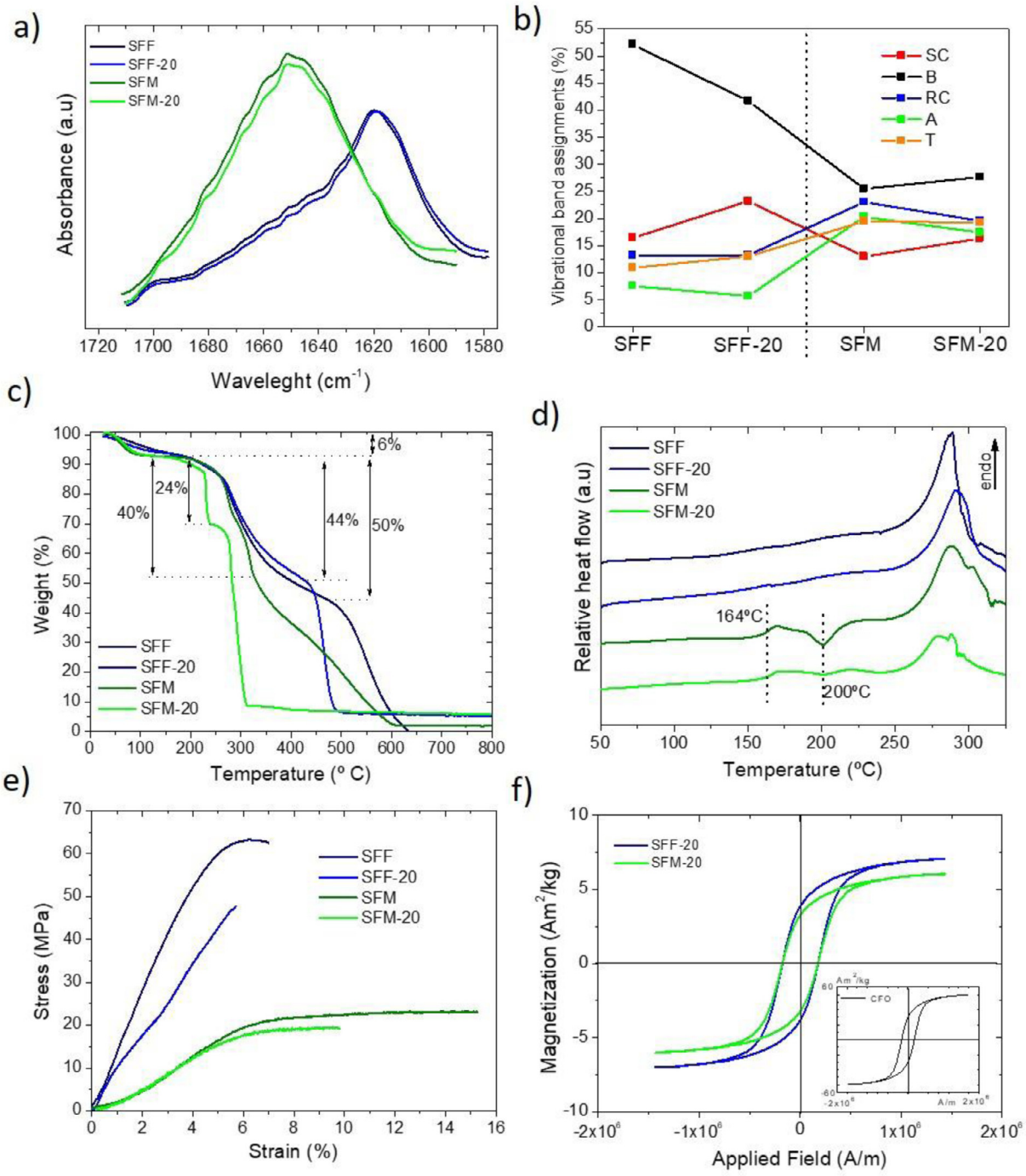

Fig. 4. Neat SFF, SFF-20, neat SFM and SFM-20 scaffolds (a) FTIR-ATR amide I spectra (b) vibrational band assignments for side chains (SC), β-Sheets (B), random coil (RC), α-helix (A) and turns (T), (c) TGA thermogravimetric curves, (d) DSC thermograms, (e) stress–strain curves and (f) magnetic hysteresis loops.

an initial weight loss at 100 ˚C corresponding to a water loss process, a second degradation from 300 to 550˚C mainly ascribed to the breakdown of SF side chain groups, the amino acid residues and the split of peptide bonds, and a final step related to the degradation of the main SF structure. After CFO NPs addition, the water lost remains equal, indicating allow effect of NPs in SF films water affinity. In contrast, the second degradation step is slightly retarded due to the addition of CFO NPs. The final degradation step, in contrast is highly affected by NPs shifting from 580 ˚C in SFF to 500 ˚C in SFF-20. The observed data are in good agreement with the FTIR data (Fig. 4(a) and (b)). Improved thermal stability by the addition of NPs in the SF matrix has been reported due to the induced transition from amorphous to crystalline phases [45]. However, this effect does not correspond to here observed FTIR results, which show the reduction of β-Sheets due to CFO NPs addition. Indeed, the slight thermal enhancement observed is in line with the proposed trapping effect of NPs on SF polypeptide chains and the induced stability [46]. Consequently, side chain groups, amino acid residues and peptide bonds breakdown are slightly reduced, improving SF thermal stability. At the same time, lowβ-Sheets formation due to NPs incorporation reduces the content of stable thermal structures, favoring the degradation of the complete structure. Final thermal degradation is also improved by the catalyst effects given by the NPs [46].

SF membranes also show the three main thermal degradation steps. The weight loss due to water evaporation is equal to that observed in films, showing allow effect of SF morphology on water affinity. However, the porous structure of the SF membranes seems to facilitate water evaporation, leading to more pronounced water loss curves. Compared with the films, no variation is observed in the first steps of second degradation. On the other hand, the side chains, amino acid residues and peptide bonds degradation and final degradation are highly affected in response to reduced β-Sheet content, which are the main responsible for the SF thermal stability [47]. The addition of CFO NPs in SF membranes does not affect the water loss process due to the low β-Sheet content of these samples, however, due to the catalytic effect of NPs, it greatly improves thermal degradation, leading to complete decomposition of SFM-20 at 300 ˚C.

DSC thermograms show the thermal transitions of SF films and membranes during heating scan from 50 to 350 ˚C (Fig. 4(d)). The curves of SFF, SFF-20, SFM and SFM-20 are presented as representative for the rest of the samples. It can be seen that during the heating process neat SF films show the characteristic thermograms of highly crystalline SF structures [26,33]. The single endothermic peak near 300˚C indicated the breakdown of SF side chains groups amino acid residues and the cleavage of peptide bonds as shown in previous TGA data (Fig. 4(c)). The CFO NPs addition to the SF films has no significant effect on the secondary structure and therefore the DSC scans remain almost invariable. However, it could be observed by DSC a slight increase in the thermal stability with the NPs addition, as the endothermic peak shifts to higher temperatures, as a result of CFO-SF interactions that affect [26].

The polypeptide chains reorganization induced by the electrospinning technique results in SF membranes with new thermal transitions (Fig. 4(d)). The increase in the number of non-ordered structures (RC) gives the peptide chains larger mobility and consequently a well-defined glass transition temperature (T_g) at 164 ˚C. Further, crystallization (T_c) at 270 ˚C appears and the peak corresponding to the degradation of peptide chains at 300 ˚C remains invariable. The incorporation of CFO NPs into SF membranes leads to similar DSC thermograms, with clear T_g and T_c transitions and degradation peaks. However, the decreased mobility of the polymer chains related to the interaction between SF chains and CFO NPs reduces the intensity of thermal transition and leads to the loss of the endothermic peak.

With respect to the mechanical properties of SF films and membranes under tensile stress, Fig. 4(e) shows the strong effect of the processing method and, therefore, sample morphology. The stress-strain curves of SFF, SFF-20, SFM and SFM-20 were used as representative for all the samples. With stress at yield values above 64 MPa, SF films show the typical behavior of non-ductile materials. Under stress, SFF shows an initial elastic region followed by a short plastic deformation until the final rupture. This behavior can be understood by the ternary configuration of SF structures. SF mainly consists on a hydrogen-bonding network of β-structured crystallites (β-sheets), responsible for the strength and rigidity of the material, and non-ordered amorphous regions (random coils), more flexible and related to its elasticity [48]. During the first deformation steps, the amorphous domains maintain all the accumulated structural force, which causes the tangled chains to unfold, leading to the elastic behavior of the film. Since the random coils are completely unwound, the deformation becomes supported by β-sheet nodes, which endure the force until their break. When CFO NPs are added, the secondary structure is slightly affected and consequently, low variation in stress–strain curves are observed (Fig. 4(e)). Lower stress on yield in the presence of CFO NPs are related to the defects induced by the NPs.

The mechanical behavior of SF electrospun membranes is characterized by fiber deformation followed by their reorientation on the direction of applied strain and finally [49], the effect on the secondary structure of the material inducing a long decrease in β-sheets formation and an increase in random structures. As a result, stress on yield values decrease to 23 MPa and elongation increases from 6% in SFF to 15% in SFM. In SFM-20 the defects induced by CFO NPs decrease both the elongation and stress at yield.

The magnetic response of the SF samples is shown in Fig. 4(f) where the hysteresis loops of SFF-20 and SFM-20 are plotted. Under the effect of the magnetic field, both SFF-20 and SFM-20 show closed hysteresis loops, similar in shape to neat CFO (insert in Fig. 4(f)). This behavior reveals that the magnetic particles preserve their original ferromagnetic behavior when placed in the SF matrix, independently of the processing procedure and, therefore, of the morphology. The saturation magnetization decreases in comparison with neat CFO NPs (7 and 6 emu g^{-1} for SFF and SFM respectively), which can be related with the matrix-filler interfacial interactions [50]. The lower saturation magnetization values observed for SFM-20 are related to the precipitation of CFO NPs during electrospinning process. Equally to neat CFO NPs, SFF-20 and SFM-20 samples show strong remanence (3.8 and 3.3 emu g^{-1} respectively) and coercivity values (both 2.2 kOe).

3.3. Bone tissue engineering applications

The SF films and membranes comprising different concentrations of CFO NPs, were further used as substrates that respond to magnetic stimuli for bone tissue en gineering, and tested for their ability to act as an active support for cell adhesion and proliferation. Initially, the biocompatibility of the substrates was measured by placing in contact the pre-osteoblasts cells with the surface of the material and by measuring their viability using MTS. The biocompatibility at different time-points was studied, namely at 24 h, 4 days and 7 days. An increased cell viability was observed with increasing the time of culture in all scaffolds, indicating that the materials are biocompatible (Fig. 5).

Also, the higher the concentration of incorporated CFO NPs, the better is cell adhesion and proliferation, a behavior that was observed for both films and membranes. The only exception was observed for SFM-20 that induced certain toxicity to the cells (Fig. 5(a)), probably due to silk biodegradability. After 7 days is acceptable that silk fibers degrade in a more extent than the films [51]. This is in good agreement with previous studies that show that the degradation of silk may be stablished after 10 days in contact with DMEM [52]. Despite silk leachable are reported to induce no toxicity or immunogenic response to the cells, in this study the biodegradation profile of silk-based structures may cause the release of CFO NPs which further induce toxicity to the cells [44].

It also should be noticed that cells grow better on the films (Fig. 5(a)) rather than on the electrospun membranes (Fig. 5(b)). In fact, between 24 h and 4 days, the cells growing on SF membranes do not experience a big increase on cell viability when compared with the cell growing over SF films. Higher cell viability in SF membranes is then observed after 7 days of culture but the results are rather low when comparted to the viability levels observed on the films. In a first assessment, smooth surfaces seems to promote better adhesion to the cells.

SF substrates were then tested for their ability to induce proliferation of pre-osteoblasts with and without magnetic stimuli. Cells growing at the surface of the nanocomposites were subjected to a magnetic stimulus or left in static conditions for 4 days, a time-point which was earlier defined as non-toxic for the cells in both substrates (Fig. 5). The cell behavior was found to be different depending on the morphology of the scaffolds as previously suggested in Fig. 5.

With the SF films, the effect of the stimuli was observed, since the proliferation rate was higher for the cells growing over the material with 10% and 20% CFO NPs subjected to the magnetic stimuli. The exception was found in the material with 5% CFO NPs and the films without NPs, which has shown the same behavior with and without stimuli, most probably due to the fact that 5% incorporated CFO NPs into the SFF are not sufficient to apply significant enough magneto-mechanical stimuli to the cells, due to the low filler content.

Regarding the electrospun membranes, no significant differences were observed in the proliferation rate of cells growing on the material subjected to the stimuli and the ones maintained under static con-

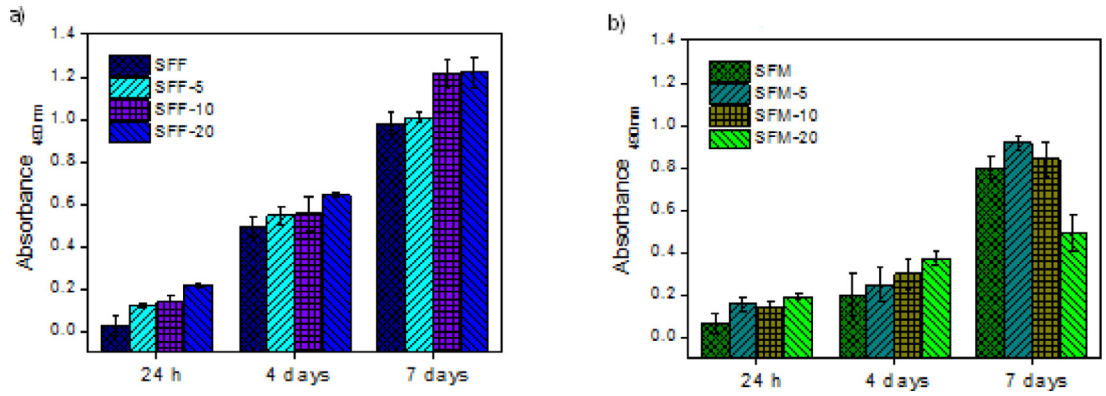

Fig. 5. Biocompatibility MTS assay on pre-osteoblasts growing on the top of (a) SF films and (b) SF membranes increasing the CFO NPs content at three time points: 24 h, 4 days and 7 days.

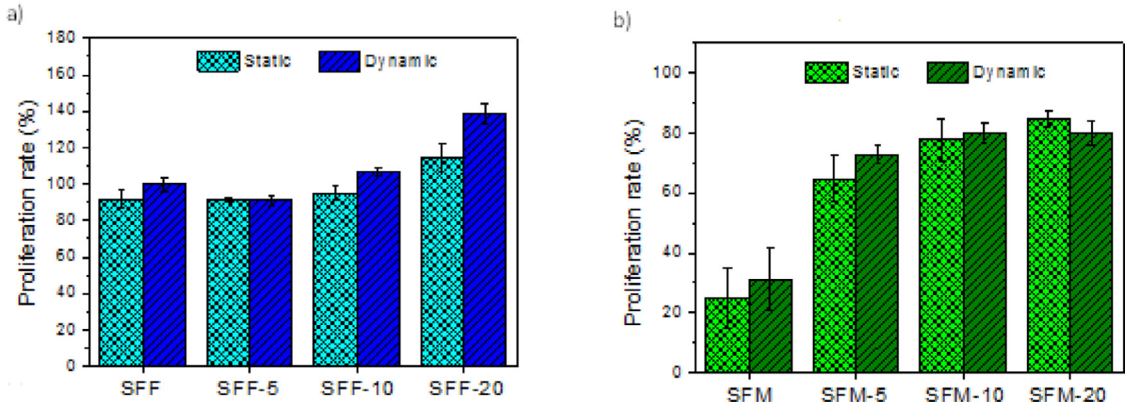

Fig. 6. Proliferation rate of pre-osteoblasts seeded on the top of (a) SF films and (b) SF electrospun membranes after 4 days with and without magnetic stimuli. The proliferation rate was calculated regarding the cells growing on the material after 24 h adhesion, just before putting in contact with the bioreactor/magnetic stimuli (see Fig. 2). The results are an average of three independent assays.

ditions. This may be indicative that these scaffolds do not induce the necessary mechanical/electrical effect on the cells (Fig. 6(a)), as previously described in other magnetic responsive materials [29,30,53]. Nevertheless, as observed in Fig. 5(a), it can be observed that a tendency for higher cellular proliferation on the scaffolds with higher concentration of NPs occurs, regardless the stimuli. This behavior indicates that the morphology of the scaffold plays an important role on the adhesion and proliferation of the cells, an effect that is, in the present case, more relevant than the magnetically induced stimuli.

To corroborate these results, the morphology of cells was visualized 4 days after cell seeding using SEM (Fig. 7). In both samples, the surface of the scaffolds was observed prior to cell seeding in order to visualize the morphology and topography of the material (Fig. 3).

In SF films, the cells seed on the surface of the material in a completely different way when compared to the membranes. While on the membranes a dense cell layer is observed, on the films the cells are round but well attached to the surface. While the rounding cells may be indicative that cells are not viable, in the herein tested films, the cells are well-attached as clearly shown by the well-stablished spider-like network around the cells and are indeed viable, as shown in Figs. 5(a) and 6(a)). The morphology observed may indicate that pre-osteoblast did not have time to differentiate into osteoblasts [54]. Under static conditions the cells seed at higher number with increased CFO NPs concentration (Fig. 7(a)), as previously observed in Fig. 6(b). Upon application of the stimuli, the cell density increases when compared to the static conditions, confirming the capability of the scaffolds to provide a proper magneto-mechanical or event local magneto-electric effect on the cells (Fig. 7(a)).

When stimulated by a magnetic bioreactor, these scaffolds induce a mechanical [29] or electrical [29,55] cue on the cells due to the magnetostriction of CFO NPs and the piezoelectricity of silk within the nanocomposites. This type of stimuli has been reported to trigger the activation of intracellular signaling cascades in a cell [56]. More specifically, the application of an electrically active microenvironment has been a strategy increasingly explored in mammalian cells. It has been stablished that electroactive materials such as piezoelectric polymers and magnetoelectric composites develop voltage at the surface of the material when a mechanical stress [57] or a magnetic field [29], respectively, is applied, thus promoting the adhesion and proliferation of eukaryotic cells, such as osteoblasts.

At static conditions, on the electrospun membranes the cells form a layer that is increasingly thicker with increasing concentration of CFO NPs (Fig. 7(b)), as previously observed in Fig. 6(b). This confirms that the morphology of the scaffold plays a key role on the proliferation of cells while the presence of CFO NPs may promote better adhesion due to the increased focal points they induce at the surface of the fibers. In fact, by observing the SEM images depicted in Fig. 7, before cell seeding, it can be observed that the CFO NPs are present at the surface of the fibers. Nevertheless, the cells growing on the membrane with 20% CFO NPs seem to be rounding up and detaching, indicating a previous state of cells death owed to the higher presence of CFO NPs.

After applying the magnetic stimuli, and despite the fact that MTS assay have shown little differences with and without the application of the stimuli, there is an increase on cell coverage over the material, mainly on the membranes with 5% and 10% CFO. The cells clearly penetrate the pores and a well-stablished cell layer is found on the surface of the

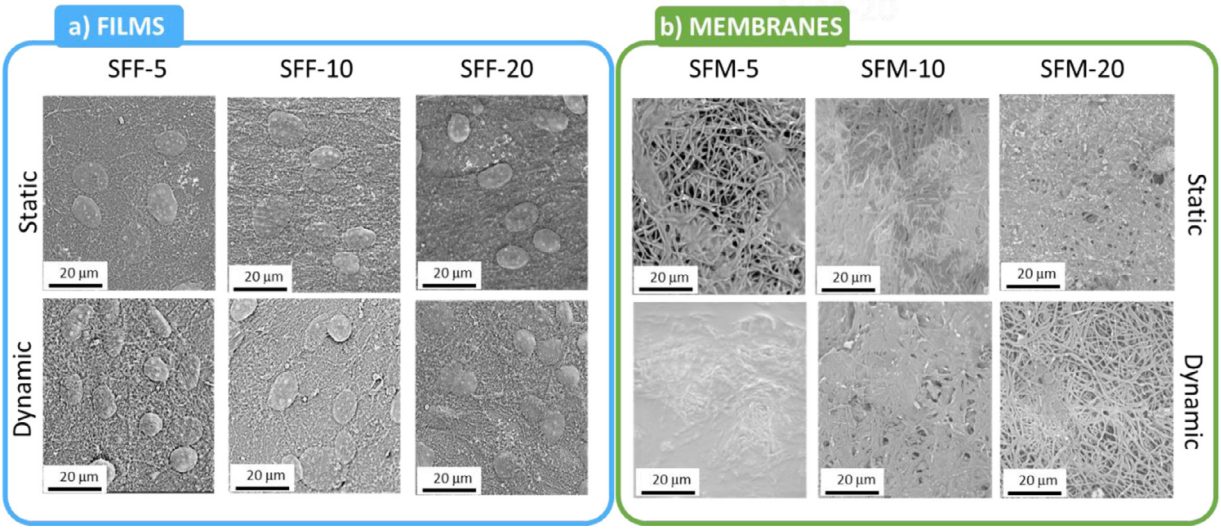

Fig. 7. SEM images of the surface of SF (a) film and (b) membranes with 5%, 10% and 20% of CFO NPs, after culture of pre-osteoblast cells for 4 days, with and without dynamic conditions.

material where the cells are intricated within the material. This effect is not so pronounced on the membrane with 20% CFO NPs.

Thus, the developed magneto-active scaffolds have been shown beneficial to improve the proliferation of cells despite the piezoelectricity of silk being different from the commonly used PVDF, where the stimuli creates an electrically active microenvironment that improves cells adhesion and proliferation [27,29,53,58–60].

Silk fibroin, by itself, has been explored for tissue engineering purposes and proven to promote osteogenesis in vitro [61] and to have osteopromotive potential in critical sized defects in vivo [62]. Therefore, the morphology of the materials also play an important role on the proliferation of pre-osteoblasts. In fact, it has been suggested that cell survival and maintenance, as well as proliferation and differentiation, are regulated by their three-dimensional microenvironment, the so called niche [63]. This specific microenvironment regulates stem cell function through several mechanisms, related with the direct contact between cells and their adjacent niche cells. Their interactions are mediated either through adherence or gap junctions, which combined with the magnetic stimuli creates the appropriate microenvironment for cell proliferation.

4. Conclusions

Silk fibroin/cobalt ferrite nanoparticles ($CoFe_2O_4$, CFO) SF/CFO composites have been prepared for tissue engineering applications by solvent-casting and electrospinning technique with different fillers content (0 wt% to 20 wt%). The CFO fillers show a good distribution within the biopolymer. The processing method affects the morphology and the subsequent roughness of the samples, as well as their the β-sheet content. For electrospun membranes, multifibrillar fibers with diameter of 850 $\pm$ 100 nm were obtained. The content of the β-sheet is independently of the filler content. All composites show good thermal and mechanical properties affected by filler content and processing technique. The magnetic behavior of these composites shows a typical ferromagnetic behavior of the CFO nanoparticles in which the magnetic response is correlated with filler content. In addition, the cell culture results show that dynamic stimulation enhanced cell viability and their morphology plays an important role in pre-osteoblast proliferation. Thus, it is demonstrated that the SF/CFO composites show excellent cell viability and can be suitable for tissue engineering applications.

Declaration of Competing Interest

The authors declare that they have no known competing financial interests or personal relationships that could have appeared to influence the work reported in this paper.

Acknowledgments

This work was supported by National funds through FCT (Fundação para a Ciência e Tecnologia) and by ERDF through COMPETE2020-Programa Operacional Competitividade e Internacionalização (POCI) in the framework of the Strategic Programs UID/FIS/04650/2019, UID/BIO/04469/2019 and projects PTDC/BTM-MAT/28237/2017 and PTDC/EMD-EMD/28159/2017. The work was also supported by FCT through project Lung Check ENMed/0049/2016. R.B.P., M.M.F. and C.M.C thanks FCT for the grant SFRH/BD/140698/2018, SFRH/BPD/121464/2016, and SFRH/BPD/112547/2015, respectively. C. Ribeiro thanks the FCT for the contract under the Stimulus of Scientific Employment (DL57/2016 junior researcher contract). Finally, the authors acknowledge funding by the Spanish Ministry of Economy and Competitiveness (MINECO) through the project MAT2016-76039-C4-3-R (AEI/FEDER, UE) and from the Basque Government Industry and Education Departments under the ELKARTEK and PIBA (PIBA-2018-06) programs, respectively. SGIker (UPV/EHU, MICINN, GV/EJ, ERDF and ESF) support is gratefully acknowledged.

Supplementary materials

Supplementary material associated with this article can be found, in the online version, at doi:10.1016/j.mtla.2020.100709.

References

[1] K. Maji, Biomaterials for bone tissue engineering: recent advances and challenges, in: B. Li, T. Webster (Eds.), Orthopedic Biomaterials, Springer, Germany, 2018, pp. 429–452.
[2] H. Jahangirian, E.G. Lemraski, R. Rafiee-Moghaddam, T.J. Webster, A review of using green chemistry methods for biomaterials in tissue engineering, Int. J. Nanomed. 13 (2018) 5953–5969, doi:10.2147/IJN.S163399.
[3] S.A. Sell, P.S. Wolfe, K. Garg, J.M. McCool, I.A. Rodriguez, G.L. Bowlin, The use of natural polymers in tissue engineering: a focus on electrospun extracellular matrix analogues, Polymers 2 (4) (2010) 522–553, doi:10.3390/polym2040522.
[4] L.-.D. Koh, Y. Cheng, C.-.P. Teng, Y.-.W. Khin, X.-.J. Loh, S.-.Y. Tee, M. Low, E. Ye, H.-.D. Yu, Y.-.W. Zhang, Structures, mechanical properties and applications of silk fibroin materials, Prog. Polym. Sci. 46 (2015) 86–110, doi:10.1016/j.progpolymsci.2015.02.001.

[5] M. Fernandes, D. Correia, A. da Costa, S. Ribeiro, M. Casal, S. Lanceros-Méndez, R. Machado, Multifunctional magnetically responsive biocomposites based on genetically engineered silk-elastin-like protein, Compos. Part B 153 (2018) 413–419, doi:10.1016/j.compositesb.2018.09.019.

[6] T. Yucel, P. Cebe, D.L. Kaplan, Structural origins of silk piezoelectricity, Adv. Funct. Mater. 21 (4) (2011) 779–785, doi:10.1002/adfm.201002077.

[7] D.N. Rockwood, R.C. Preda, T. Yücel, X. Wang, M.L. Lovett, D.L. Kaplan, Materials fabrication from Bombyx mori silk fibroin, Nat. Protoc. 6 (10) (2011) 1612, doi:10.1038/nprot.2011.379.

[8] Y. Cheng, L.-.D. Koh, D. Li, B. Ji, M.-.Y. Han, Y.-.W. Zhang, On the strength of β-sheet crystallites of Bombyx mori silk fibroin, J. R. Soc. Interface 11 (96) (2014) 20140305, doi:10.1098/rsif.2014.0305.

[9] Y. Takasu, H. Yamada, K. Tsubouchi, Isolation of three main sericin components from the cocoon of the silkworm, Bombyx mori, Biosci. Biotechnol. Biochem. 66 (12) (2002) 2715–2718, doi:10.1271/bbb.66.2715.

[10] F.A. Sheikh, H.W. Ju, J.M. Lee, B.M. Moon, H.J. Park, O.J. Lee, J.-.H. Kim, D.-.K. Kim, C.H. Park, 3D electrospun silk fibroin nanofibers for fabrication of artificial skin, Nanomed.: Nanotechnol. Biol. Med. 11 (3) (2015) 681–691, doi:10.1016/j.nano.2014.11.007.

[11] B.-.M. Min, G. Lee, S.H. Kim, Y.S. Nam, T.S. Lee, W.H. Park, Electrospinning of silk fibroin nanofibers and its effect on the adhesion and spreading of normal human keratinocytes and fibroblasts in vitro, Biomaterials 25 (7–8) (2004) 1289–1297, doi:10.1016/j.biomaterials.2003.08.045.

[12] B. Kundu, R. Rajkhowa, S.C. Kundu, X. Wang, Silk fibroin biomaterials for tissue regenerations, Adv. Drug Deliv. Rev. 65 (4) (2013) 457–470, doi:10.1016/j.addr.2012.09.043.

[13] H.W. Ju, O.J. Lee, J.M. Lee, B.M. Moon, H.J. Park, Y.R. Park, M.C. Lee, S.H. Kim, J.R. Chao, C.S. Ki, Wound healing effect of electrospun silk fibroin nanomatrix in burn-model, Int. J. Biol. Macromol. 85 (2016) 29–39, doi:10.1016/j.ijbiomac.2015.12.055.

[14] P. Ke, X.-.N. Jiao, X.-.H. Ge, W.-.M. Xiao, B. Yu, From macro to micro: structural biomimetic materials by electrospinning, RSC Adv. 4 (75) (2014) 39704–39724, doi:10.1039/C4RA05098C.

[15] S. Ramakrishna, W.-.E. Teo, T.-.C. Lim, Z. Ma, An Introduction to Electrospinning and Nanofibers, World Scientific, 2005, doi:10.1142/5894.

[16] Q.P. Pham, U. Sharma, A.G. Mikos, Electrospinning of polymeric nanofibers for tissue engineering applications: a review, Tissue Eng. 12 (5) (2006) 1197–1211, doi:10.1089/ten.2006.12.1197.

[17] T. Jiang, E.J. Carbone, K.W.-H. Lo, C.T. Laurencin, Electrospinning of polymer nanofibers for tissue regeneration, Prog. Polym. Sci. 46 (2015) 1–24, doi:10.1016/j.progpolymsci.2014.12.001.

[18] S. Khorshidi, A. Solouk, H. Mirzadeh, S. Mazinani, J.M. Lagaron, S. Sharifi, S. Ramakrishna, A review of key challenges of electrospun scaffolds for tissue-engineering applications, J. Tissue Eng. Regen. Med. 10 (9) (2016) 715–738, doi:10.1002/term.1978.

[19] F. Zamani, M. Amani-Tehran, M. Latifi, M.A. Shokrgozar, The influence of surface nanoroughness of electrospun PLGA nanofibrous scaffold on nerve cell adhesion and proliferation, J. Mater. Sci.: Mater. Med. 24 (6) (2013) 1551–1560, doi:10.1007/s10856-013-4905-6.

[20] S. Megelski, J.S. Stephens, D.B. Chase, J.F. Rabolt, Micro-and nanostructured surface morphology on electrospun polymer fibers, Macromolecules 35 (22) (2002) 8456–8466, doi:10.1021/ma020444a.

[21] F.T. Moutos, L.E. Freed, F. Guilak, A biomimetic three-dimensional woven composite scaffold for functional tissue engineering of cartilage, Nat. Mater. 6 (2) (2007) 162, doi:10.1038/nmat1822.

[22] W. Cui, Y. Zhou, J. Chang, Electrospun nanofibrous materials for tissue engineering and drug delivery, Sci. Technol. Adv. Mater. 11 (1) (2010) 014108, doi:10.1088/1468-6996/11/1/014108.

[23] E. Díaz, M. Valle, S. Ribeiro, S. Lanceros-Mendez, J. Barandiarán, Development of magnetically active scaffolds for bone regeneration, Nanomaterials 8 (9) (2018) 678, doi:10.3390/nano8090678.

[24] V.F. Cardoso, A. Francesko, C. Ribeiro, M. Bañobre-López, P. Martins, S. Lanceros-Mendez, Advances in magnetic nanoparticles for biomedical applications, Adv. Healthcare Mater. 7 (5) (2018) 1700845, doi:10.1002/adhm.201700845.

[25] R. Brito-Pereira, D. Correia, C. Ribeiro, A. Francesko, I. Etxebarria, L. Pérez-Álvarez, J. Vilas, P. Martins, S. Lanceros-Mendez, Silk fibroin-magnetic hybrid composite electrospun fibers for tissue engineering applications, Compos. Part B 141 (2018) 70–75, doi:10.1016/j.compositesb.2017.12.046.

[26] A. Reizabal, S. Gonçalves, R. Brito-Pereira, P. Costa, C.M. Costa, L. Pérez-Álvarez, J.L. Vilas-Vilela, S. Lanceros-Méndez, Optimized silk fibroin piezoresistive nanocomposites for pressure sensing applications based on natural polymers, Nanoscale Adv. 1 (2019) 2284–2292, doi:10.1039/C8NA00417J.

[27] C. Ribeiro, V. Sencadas, D.M. Correia, S. Lanceros-Méndez, Piezoelectric polymers as biomaterials for tissue engineering applications, Colloids Surf., B 136 (2015) 46–55, doi:10.1016/j.colsurfb.2015.08.043.

[28] P. Martins, S. Ribeiro, C. Ribeiro, V. Sencadas, A. Gomes, F. Gama, S. Lanceros-Méndez, Effect of poling state and morphology of piezoelectric poly (vinylidene fluoride) membranes for skeletal muscle tissue engineering, RSC Adv. 3 (39) (2013) 17938–17944, doi:10.1039/C3RA43499K.

[29] C. Ribeiro, V. Correia, P. Martins, F.M. Gama, S. Lanceros-Mendez, Proving the suitability of magnetoelectric stimuli for tissue engineering applications, Colloids Surf., B 140 (2016) 430–436, doi:10.1016/j.colsurfb.2015.12.055.

[30] M.M. Fernandes, D.M. Correia, C. Ribeiro, N. Castro, V. Correia, S. Lanceros-Mendez, Bioinspired three-dimensional magneto-active scaffolds for bone tissue engineering, ACS Appl. Mater. Interfaces 11 (2019) 45265–45275, doi:10.1021/acsami.9b14001.

[31] S. Zhang, M. Prabhakaran, S. Ramakrishna, W. Swieszkowski, Nano-engineered biocomposite tricomponent polymer based matrices for bone tissue engineering, Int. J. Polym. Mater. Polym. Biomater. 65 (2016) 807–815, doi:10.1080/00914037.2016.1163561.

[32] M. Kooti, M. Afshari, Magnetic cobalt ferrite nanoparticles as an efficient catalyst for oxidation of alkenes, Sci. Iran 19 (6) (2012) 1991–1995, doi:10.1016/j.scient.2012.05.005.

[33] A. Reizabal, D.M. Correia, C.M. Costa, L. Perez-Alvarez, J.L. Vilas-Vilela, S. Lanceros-Méndez, Silk fibroin bending actuators as an approach toward natural polymer based active materials, ACS Appl. Mater. Interfaces 11 (33) (2019) 30197–30206, doi:10.1021/acsami.9b07533.

[34] X. Yuan, D.E. Arkonac, P.-h.G. Chao, G. Vunjak-Novakovic, Electrical stimulation enhances cell migration and integrative repair in the meniscus, Sci. Rep. 4 (2014) 3674, doi:10.1038/srep03674.

[35] P. Martins, A. Lasheras, J. Gutierrez, J.M. Barandiaran, I. Orue, S. Lanceros-Mendez, Optimizing piezoelectric and magnetoelectric responses on $CoFe_2O_4$/P(VDF-TrFE) nanocomposites, J. Phys. D: Appl. Phys. 44 (49) (2011) 495303, doi:10.1088/0022-3727/44/49/495303.

[36] X. Zhu, J. Chen, L. Scheideler, R. Reichl, J. Geis-Gerstorfer, Effects of topography and composition of titanium surface oxides on osteoblast responses, Biomaterials 25 (18) (2004) 4087–4103, doi:10.1016/j.biomaterials.2003.11.011.

[37] J.I. Rosales-Leal, M.A. Rodríguez-Valverde, G. Mazzaglia, P.J. Ramón-Torregrosa, L. Díaz-Rodríguez, O. García-Martínez, M. Vallecillo-Capilla, C. Ruiz, M.A. Cabrerizo-Vílchez, Effect of roughness, wettability and morphology of engineered titanium surfaces on osteoblast-like cell adhesion, Colloids Surf. A 365 (1) (2010) 222–229, doi:10.1016/j.colsurfa.2009.12.017.

[38] K.E. Strawhecker, S.K. Kumar, J.F. Douglas, A. Karim, The critical role of solvent evaporation on the roughness of spin-cast polymer films, Macromolecules 34 (14) (2001) 4669–4672, doi:10.1021/ma001440d.

[39] F. Abdel-Hady, A. Alzahrany, M. Hamed, Experimental validation of upward electrospinning process, ISRN Nanotechnol. (2011) (2011) Article ID 851317, 14 pages, doi:10.5402/2011/851317.

[40] A.L. Yarin, S. Koombhongse, D.H. Reneker, Bending instability in electrospinning of nanofibers, J. Appl. Phys. 89 (5) (2001) 3018–3026, doi:10.1063/1.1333035.

[41] A.L. Yarin, W. Kataphinan, D.H. Reneker, Branching in electrospinning of nanofibers, J. Appl. Phys. 98 (6) (2005) 064501, doi:10.1063/1.2060928.

[42] I.C. Um, H.Y. Kweon, K.G. Lee, Y.H. Park, The role of formic acid in solution stability and crystallization of silk protein polymer, Int. J. Biol. Macromol. 33 (4) (2003) 203–213, doi:10.1016/j.ijbiomac.2003.08.004.

[43] S. Mohapatra, S.R. Rout, S. Maiti, T.K. Maiti, A.B. Panda, Monodisperse mesoporous cobalt ferrite nanoparticles: synthesis and application in targeted delivery of antitumor drugs, J. Mater. Chem. 21 (25) (2011) 9185–9193, doi:10.1039/C1JM10732A.

[44] F. Ahmad, X. Liu, Y. Zhou, H. Yao, An in vivo evaluation of acute toxicity of cobalt ferrite ($CoFe_2O_4$) nanoparticles in larval-embryo Zebrafish (Danio rerio), Aquat. Toxicol. 166 (2015) 21–28, doi:10.1016/j.aquatox.2015.07.003.

[45] X.-.X. Feng, L.-.L. Zhang, J.-.Y. Chen, Y.-.H. Guo, H.-.P. Zhang, C.-.I. Jia, Preparation and characterization of novel nanocomposite films formed from silk fibroin and nano-TiO_2, Int. J. Biol. Macromol. 40 (2) (2007) 105–111, doi:10.1016/j.ijbiomac.2006.06.011.

[46] K. Chrissafis, D. Bikiaris, Can nanoparticles really enhance thermal stability of polymers? Part I: an overview on thermal decomposition of addition polymers, Thermochim. Acta 523 (1) (2011) 1–24, doi:10.1016/j.tca.2011.06.010.

[47] K. Yazawa, K. Ishida, H. Masunaga, T. Hikima, K. Numata, Influence of water content on the β-sheet formation, thermal stability, water removal, and mechanical properties of silk materials, Biomacromolecules 17 (3) (2016) 1057–1066, doi:10.1021/acs.biomac.5b01685.

[48] Y.-.X. He, N.-.N. Zhang, W.-.F. Li, N. Jia, B.-.Y. Chen, K. Zhou, J. Zhang, Y. Chen, C.-.Z. Zhou, N-terminal domain of bombyx mori fibroin mediates the assembly of silk in response to pH decrease, J. Mol. Biol. 418 (3) (2012) 197–207, doi:10.1016/j.jmb.2012.02.040.

[49] M.M. Maciel, S. Ribeiro, C. Ribeiro, A. Francesko, A. Maceiras, J.L. Vilas, S. Lanceros-Méndez, Relation between fiber orientation and mechanical properties of nano-engineered poly(vinylidene fluoride) electrospun composite fiber mats, Compos. Part B 139 (2018) 146–154, doi:10.1016/j.compositesb.2017.11.065.

[50] Z. Guo, S. Park, H.T. Hahn, S. Wei, M. Moldovan, A.B. Karki, D.P. Young, Magnetic and electromagnetic evaluation of the magnetic nanoparticle filled polyurethane nanocomposites, J. Appl. Phys. 101 (9) (2007) 09M511, doi:10.1063/1.2711074.

[51] Y. Cao, B. Wang, Biodegradation of silk biomaterials, Int. J. Mol. Sci. 10 (2009) 1514–1524, doi:10.3390/ijms10041514.

[52] O.J. Lee, J.M. Lee, J. Heui Kim, J. Kim, H. Kweon, Y. Young Jo, C. Park, Biodegradation behavior of silk fibroin membranes in repairing tympanic membrane perforations, J. Biomed. Mater. Res. Part A 100 (2012) 2018–2026, doi:10.1002/jbm.a.33308.

[53] C. Ribeiro, S. Moreira, V. Correia, V. Sencadas, J.G. Rocha, F.M. Gama, J.L.G. Ribelles, S. Lanceros-Mendez, Enhanced proliferation of pre-osteoblastic cells by dynamic piezoelectric stimulation, RSC Adv. 2 (30) (2012) 11504–11509, doi:10.1039/C2RA21841K.

[54] T.A. Franz-Odendaal, B.K. Hall, P.E. Witten, Buried alive: how osteoblasts become osteocytes, Dev. Dyn. 235 (1) (2006) 176–190, doi:10.1002/dvdy.20603.

[55] R. Gonçalves, P. Martins, X. Moya, M. Ghidini, V. Sencadas, G. Botelho, N.D. Mathur, S. Lanceros-Mendez, Magnetoelectric $CoFe_2O_4$/polyvinylidene fluoride electrospun nanofibres, Nanoscale 7 (17) (2015) 8058–8061, doi:10.1039/C5NR00453E.

[56] M. Aizawa, S. Koyama, K. Kimura, T. Haruyama, Y. Yanagida, E. Kobatake, Electrically stimulated modulation of cellular function in proliferation, differentiation, and gene expression, Electrochemistry 67 (1999) 118–125, doi:10.5796/electrochemistry.67.118.

[57] C. Ribeiro, D.M. Correia, S. Ribeiro, V. Sencadas, G. Botelho, S. Lanceros-Méndez, Piezoelectric poly(vinylidene fluoride) microstructure and poling state in active tissue engineering, Eng. Life Sci. 15 (4) (2015) 351–356, doi:10.1002/elsc.201400144.
[58] C. Ribeiro, J. Pärssinen, V. Sencadas, V. Correia, S. Miettinen, V.P. Hytönen, S. Lanceros-Méndez, Dynamic piezoelectric stimulation enhances osteogenic differentiation of human adipose stem cells, J. Biomed. Mater. Res. 103 (6) (2015) 2172–2175 Part A, doi:10.1002/jbm.a.35368.
[59] C. Ribeiro, J.A. Panadero, V. Sencadas, S. Lanceros-Méndez, M.N. Tamaño, D. Moratal, M. Salmerón-Sánchez, J.L. Gómez Ribelles, Fibronectin adsorption and cell response on electroactive poly(vinylidene fluoride) films, Biomed. Mater. 7 (3) (2012) 035004–035013, doi:10.1088/1748-6041/7/3/035004.
[60] C. Ribeiro, C.M. Costa, D.M. Correia, J. Nunes-Pereira, J. Oliveira, P. Martins, R. Gonçalves, V.F. Cardoso, S. Lanceros-Méndez, Electroactive poly(vinylidene fluoride)-based structures for advanced applications, Nat. Protoc. 13 (2018) 681–704, doi:10.1038/nprot.2017.157.
[61] H.J. Kim, U.-.J. Kim, G.G. Leisk, C. Bayan, I. Georgakoudi, D.L. Kaplan, Bone regeneration on macroporous aqueous-derived silk 3-D scaffolds, Macromol. Biosci. 7 (5) (2007) 643–655, doi:10.1002/mabi.200700030.
[62] L. Meinel, O. Betz, R. Fajardo, S. Hofmann, A. Nazarian, E. Cory, M. Hilbe, J. McCool, R. Langer, G. Vunjak-Novakovic, H.P. Merkle, B. Rechenberg, D.L. Kaplan, C. Kirker-Head, Silk based biomaterials to heal critical sized femur defects, Bone 39 (4) (2006) 922–931, doi:10.1016/j.bone.2006.04.019.
[63] M. Votteler, P.J. Kluger, H. Walles, K. Schenke-Layland, Stem cell microenvironments – unveiling the secret of how stem cell fate is defined, Macromol. Biosci. 10 (11) (2010) 1302–1315, doi:10.1002/mabi.201000102.